

## MODELING AND NUMERICAL ANALYSIS OF THE TWO-PHASE GEOTHERMAL RESERVOIR AT OGIRI, KYUSHU, JAPAN

Yurie Kumamoto<sup>a</sup>, Ryuichi Itoi<sup>a</sup>, Toshiaki Tanaka<sup>a</sup> and Yukio Hazama<sup>b</sup>

<sup>a</sup> Department of Earth Resources Engineering, Kyushu University  
744, Motoooka, Nishi-ku, Fukuoka, 819-0395, Japan

<sup>b</sup> Nittetsu Kagoshima Geothermal Co.  
4-2-3, Shiba, Minato-ku, Tokyo, 108-0014, Japan  
yurie-kumamoto@mine.kyushu-u.ac.jp

### **ABSTRACT**

The Ogiri geothermal system is characterized with the presence of steam-water two-phase zone and the fractured zone along Ginyu Fault which is the main target. For representing these characters, a numerical reservoir model has been developed. In the present study, we applied the MINC method to the grid blocks corresponding to the production zone of numerical model and carried out the history matching simulation with the model by using the code TOUGH2 (Pruess et al, 1999).

### **1. INTRODUCTION**

The Ogiri geothermal power plant located in the West Kirishima area was opened in early 1996. Nittetsu Kagoshima Geothermal Co. (NKGK) supplies the geothermal steam to the power plant with installed capacity of 30 MWe that has been operated by the Kyushu Electric Power Co. In the exploitation stage in the West Kirishima area, 50 exploratory wells were drilled (Goko, 2000) and 10 production wells and 7 reinjection wells were completed when the power plant started its operation (Japan Geothermal Energy Association, 2000). At present, the numbers of production and reinjection wells are 14 and 9, respectively. The steam production rate is approximately 275 t/h and the separated hot water for reinjection is 875 t/h at the separation pressure of 0.24 MPa (Japan Geothermal Energy Association, 2000). The power plant maintains a high utilization efficiency of 94.4% as of June, 2007 (Personal communication, 2007).

Steam production rate has continuously decreased since the power plant was started. Therefore, a numerical reservoir model is developed for analyzing reservoir behaviors upon full production, finding the causes of decline and forecasting future reservoir performances. Development of the numerical reservoir model for the field has significant challenges because the field has two complicated

characteristics. Firstly, fractured geothermal reservoir is likely developed along Ginyu Fault which is the main production zone in the field. Secondary, the geothermal system consists of a two-phase upper reservoir overlying a hot-water reservoir.

Kumamoto et al. (2008a, b) developed a numerical reservoir model of the field both in its preexploitation and exploitation, using the iTOUGH2 (Finsterle, 2000) and the TOUGH2 numerical simulators (Pruess et al., 1999). In these studies, we developed a three-dimensional numerical reservoir model of porous-type and carried out natural-state and history matching simulations. The optimum values of rock permeabilities in the field were estimated successfully by using iTOUGH2. This model succeeded to reproduce a two-phase zone formed in the shallow layers of the Ogiri system. Simulated results provided a good overall match to measured downhole pressure and temperature histories of the one observation well and enthalpy histories of production wells whose feed zone locates in hot water dominated reservoir during the history matching simulation. However, the simulated results showed a rather poor match with these measurements of wells located in the vapor dominated zone.

In these backgrounds, we developed a numerical model of the fractured geothermal reservoir for the Ogiri field and carried out the history matching simulation with the model. The model was calibrated with the code TOUGH2. For modeling a fractured zone in the Ogiri system, we employed the MINC method (Pruess, 1983). The newly developed reservoir model of Ogiri provided a better overall match to the measured data in the vapor-dominated wells. Moreover, the impacts of the matrix permeabilities of the fractured geothermal reservoir models on simulated results were examined.

### **2. GEOLOGICAL SETTING**

The Ogiri geothermal field is situated in the West Kirishima geothermal area, at an elevation of 700m

to 900m above sea level (a.s.l) on the western flank of Kirishima volcano in southern Kyushu. The geological map and the geological cross section of this area are shown in Figures 1 and 2. The basement rock is the Cretaceous Shimanto Group composed mainly of sandstone and shale. Quaternary andesitic lavas and pyroclastic flow deposits with a small amount of lacustrine sediments unconformably overlie the Shimanto Group (NEDO, 1983; 1987; Taguchi et al., 1983; Imura and Kobayashi, 2001). The volcanic rocks consist mainly of pyroxene andesite with minor amounts of hornblende andesite

(Goko, 2000). Many hydrothermal alteration zones are found in the West Kirishima geothermal area (Kodama and Nakajima, 1988; Goko, 2000). In general, these zones are aligned along ENE-WSW and NW-SE directions, and they are interlaced. Distribution of alteration zones matches relatively well with the lineament in this area. This characteristic points out that the fracture system at deep zone controls the formation of the alteration zones. Table 1 summarizes hydrogeological features of each formation in the Ogiri geothermal system.

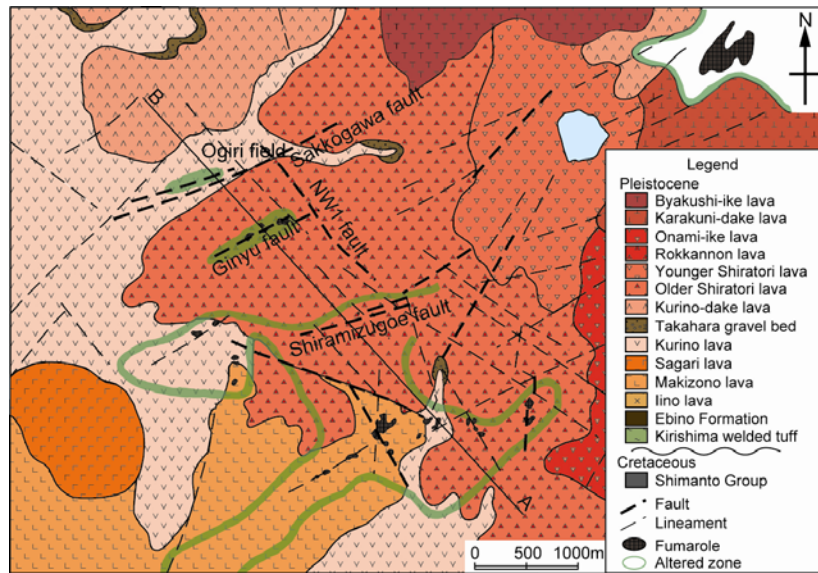


Figure 1: Geological map of the West Kirishima area (modified from Goko (1995, 2000))

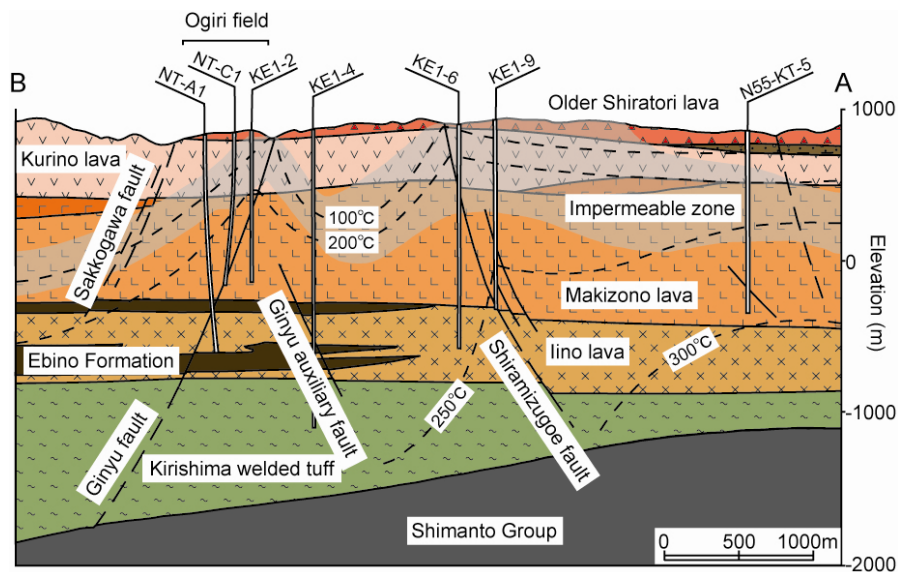


Figure 2: Geological cross section along A-B line in Fig.1 of the West Kirishima geothermal area (modified from Goko (1995, 2000))

Table 1: Hydrogeological features of formation in the Ogiri geothermal system (modified from Kodama and Nakajima (1988))

Name of formation	Hydrogeological feature
Older Shiratori lava – Sagari lava	<ul style="list-style-type: none"> <li>● Permeable with fractures such as joint</li> </ul>
Makizono lava (Upper part – Middle part)	<ul style="list-style-type: none"> <li>● Fractures are cemented by alternation mineral.</li> <li>● Play as cap rock</li> </ul>
Makizono lava (Lower part) – Kirishima welded tuff (Volcanic conglomerate)	<ul style="list-style-type: none"> <li>● Fractures are well-developed.</li> <li>● Main reservoir</li> </ul>
Kirishima welded tuffs	<ul style="list-style-type: none"> <li>● Scarce fracture</li> <li>● Presence of faults as the flow path of geothermal fluid</li> </ul>
Shimanto Group	<ul style="list-style-type: none"> <li>● Presence of fracture</li> <li>● Geothermal fluid has been stored.</li> </ul>

### 3. CONCEPTUAL MODEL

Kodama and Nakajima (1988) and Goko (2004) reported a detailed account of the subsurface temperature structure of the West Kirishima geothermal area including Ogiri geothermal field. The temperature at depth tends to increase from west to east and south-east toward the center of the Kirishima volcanoes. The heat sources of the West Kirishima geothermal area is considered to have been formed by the volcanic activity of Kirishima volcanoes which started volcanic activities about 0.6 Ma ago (Goko, 2004). Vertical profiles of the wells sited along Ginyu Fault indicate that temperature gradually increases from ground surface to 500m a.s.l. Then, temperature increases sharply with high gradient between 500m and 200m a.s.l. which implies that conductive heat transfer is dominant. Below this zone, temperature shows a relatively uniform value of 230°C (Kodama and Nakajima, 1988). In particular, the well bottom temperature in Well N56-KT-8 situated in the southeastern part of the West Kirishima area reached about 300°C at a depth of 1800m (765m b.s.l.).

The Ginyu hot spring is located in the southern part of Ogiri and fumaroles are found along Ginyu Fault. Kodama and Nakajima (1988) pointed out the heat discharge from the ground surface of the hot spring is approximately 12800 kJ/s.

According to the observed data of the Ogiri geothermal field, the geothermal system is composed of a two-phase upper reservoir overlying a hot-water reservoir. The two-phase zone is considered to have extended with exploitation. A low permeability confining layer separates the geothermal reservoir

composed by the two-phase zone and single-phase zone from the shallow groundwater aquifer.

The Ogiri area is characterized by the presence of Ginyu, Ginyu auxiliary and Sakkogawa Faults. Moreover, the NW1 Fault which intersects with Ginyu, Ginyu auxiliary and Sakkogawa Faults is also found. The locations of each fault are shown in Figure 1. The characteristics of each fault are summarized in Table 2.

Table 2: Characteristics of faults in the Ogiri geothermal area

Name of fault	Characteristic
Ginyu Fault	<ul style="list-style-type: none"> <li>● ENE-WSW trend</li> <li>● Main reservoir targeted for development</li> <li>● Nearly-planar fracture</li> <li>● Uniform temperature of 230°C</li> <li>● Formation of a two-phase zone in the shallow part</li> </ul>
Ginyu auxiliary Fault	<ul style="list-style-type: none"> <li>● ENE-WSW trend with south dip</li> <li>● Temperature distribution with range from 220°C and 240°C</li> <li>● High potential to be target for development</li> </ul>
Sakkogawa Fault	<ul style="list-style-type: none"> <li>● ENE-WSW trend</li> <li>● Flow path of meteoric water</li> </ul>
NW1 Fault	<ul style="list-style-type: none"> <li>● NW - SE trend</li> <li>● Flow path of the geothermal fluid supplied from deep zone</li> </ul>

### 4. NUMERICAL SIMULATION

#### 4-1. Grid system

The Ogiri reservoir was modeled by a three-dimensional grid system that covers an area of 5.5 km by 3.9 km with elevation 250 m a.s.l. down to 2600 m b.s.l. The model was divided on a horizontal plane into 23 blocks for east-west and 11 blocks for south-north directions with seven layers. The layers were named from AA to GG which represent the top and the bottom layers of the grid system, respectively. We used the codes Mulgeom and Mulgraph (O'Sullivan and Bullivant, 1995) as pre- and post- data processors. Table 3 summarizes information of horizontal layers used in the computational grid. The total number of the grid blocks is 1771. The sizes of the grid blocks have a range from 100m×100m to 3000 m×3000 m with thicknesses of 100 m to 1600 m. The smallest blocks were used in areas corresponding to the faults, while larger blocks were employed in outer regions. The grid system was tilted by 27° from the east to north because the main fault systems in ENE – SWS directions can be represented properly with

rectangular coordinates. Figure 3 sketches the plan view of the model corresponding to the domain in which observed data and calculated values are compared.

Eleven rock types were employed in the model to assign different rock properties for the grid blocks. We determined the distributions of rock types in the numerical model on the basis of the hydrogeological characteristics of the Ogiri geothermal field. A vertical slice of the grid system corresponding to the geological cross section (Figure 2) is shown in Figure 4. Table 4 summarizes permeability values and thermal conductivity of each rock type assigned to the numerical model. Kumamoto et al. (2008a) carried out simulation studies for estimating the rock properties of the model for Ogiri in detail. The optimum values of rock permeability in the model were estimated through inverse analysis by using the code iTOUGH2 (Finsterle, 2000), therefore those values were used here in constructing the numerical model. Porosity of 10%, density of 2500 kg/m<sup>3</sup> and specific heat of 1050 J/kg · °C were given to all rock types.

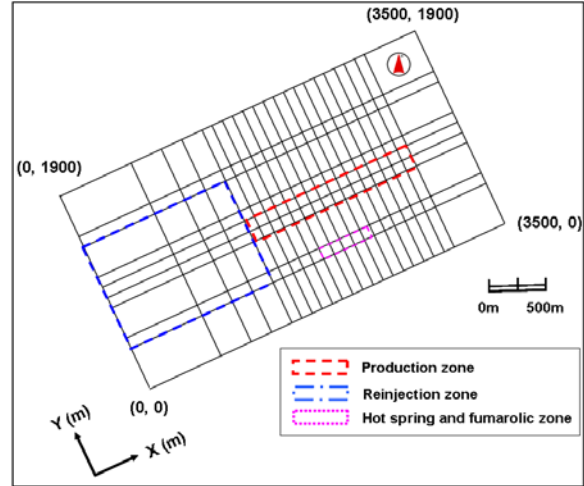


Figure 3: Plan view of the numerical model, with close-up of the domain in which observed data and calculated values are compared

**Table 3: Vertical grid geometry**

Name of layer	Depth (m b.s.l.)	Thickness (m)	Depth of block center (m b.s.l.)
Top		Infinite	
AA	-250 - 0	250	-175
BB	0 - 100	100	50
CC	100 - 200	100	150
DD	200 - 400	200	300
EE	400 - 600	200	500
FF	600 - 1000	400	800
GG	1000 - 2600	1600	1800

Table 4: Rock properties of the numerical model

Rock Type	Permeability (m <sup>2</sup> )		Thermal conductivity (W/m <sup>2</sup> C)
	kx, ky	kz	
Ginyu fault (Production area)	$3.70 \times 10^{-13}$	$1.21 \times 10^{-13}$	2.6
Ginyu fault (Reinjection area)	$3.36 \times 10^{-14}$	$3.16 \times 10^{-16}$	2.6
Ginyu auxiliary fault	$3.16 \times 10^{-16}$	$2.03 \times 10^{-14}$	2.6
Sakkogawa fault	$3.16 \times 10^{-16}$	$3.16 \times 10^{-19}$	2.6
NW1 fault	$3.81 \times 10^{-14}$	$7.23 \times 10^{-15}$	2.6
Impermeable zone (Cap rock)	$1.70 \times 10^{-18}$	$3.56 \times 10^{-19}$	1.5
Makizono lava (Upper part)	$2.98 \times 10^{-15}$	$3.34 \times 10^{-19}$	1.5
Makizono lava (Lower part)	$4.95 \times 10^{-15}$	$8.06 \times 10^{-15}$	2.6
Iino lava	$2.89 \times 10^{-16}$	$1.17 \times 10^{-15}$	2.6
Basement rock (Shimanto Group)	$2.56 \times 10^{-18}$	$1.00 \times 10^{-14}$	3.0
Top layer	$1.70 \times 10^{-18}$	$3.56 \times 10^{-19}$	1.5

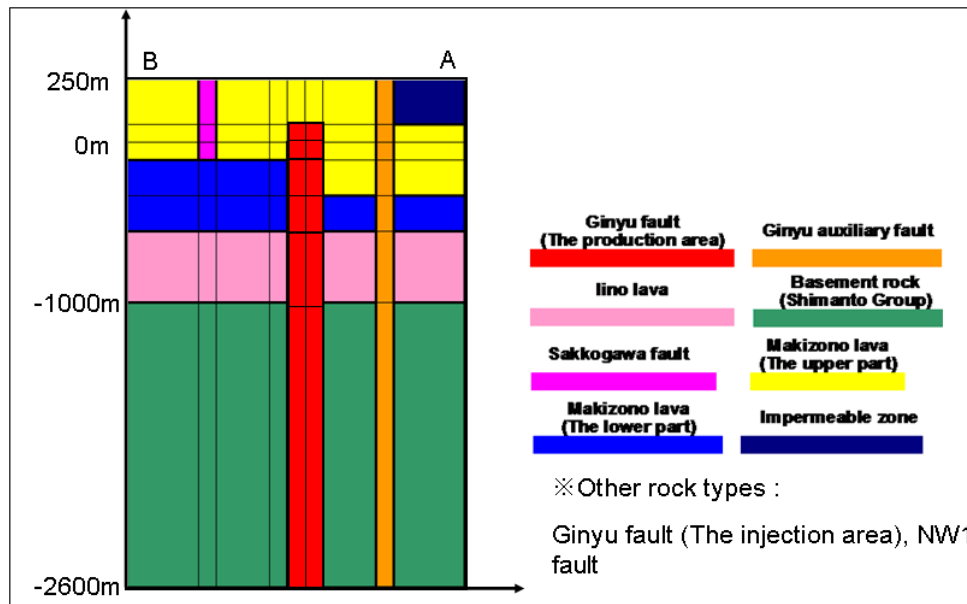


Figure 4: Vertical slice of the numerical model, with close-up of the domain in which measured and simulated values are compared

#### 4-2. MINC model

We applied the MINC method to the grid blocks that represent main production zone of Ginyu Fault as shown in Figure 5. The MINC method has been reported in detail by Pruess et al. (1999) together with its effectiveness for representing a coupled fluid and heat flow in fractured media in a numerical model. We first examined its effectiveness in the numerical model by applying the MINC process for all grid blocks corresponding to Ginyu Fault except the layer AA. However, steam-water two-phase zone was formed only in the shallow layers and water single phase remains in other deeper layers throughout the simulation period. Thus, the MINC method was applied only to the BB and CC layers in the model because of saving computation time. Table 5 summarizes parameter values used in simulations. When the MINC method is employed in the numerical model, the permeability of matrix plays an important role (Pruess, 1983). The smaller the permeability of matrix, the less the amount of fluid flows into fracture space. Then conductive heat transport from matrix into fracture space may cause an increase of fluid enthalpy in the void space. Once two-phase zone is formed in the fracture space, insufficient supply of fluid from matrix into fracture

results in significant drops in pressure and temperature in fracture zone. In particular, the effects become significant when the matrix permeability is below  $10^{-15} \text{ m}^2$ . Therefore, we carried out numerical simulation by assigning 4 different matrix permeabilities;  $10^{-15} \text{ m}^2$ ,  $10^{-16} \text{ m}^2$ ,  $10^{-17} \text{ m}^2$  and  $10^{-18} \text{ m}^2$ . These constructed models are denoted as MINC models in the later section.

Table 5: Parameters employed in simulation work

Matrix	
Permeability	$k_m = 10^{-15} \text{ m}^2, 10^{-16} \text{ m}^2, 10^{-17} \text{ m}^2, 10^{-18} \text{ m}^2$
Porosity	$\phi_m = 10 \%$
Fracture	
Permeability	$k_{fx} = 3.70 \times 10^{-13} \text{ m}^2, k_{fy} = 1.21 \times 10^{-13} \text{ m}^2$
Porosity	$\phi_f = 50 \%$
Spacing	$\lambda = 50 \text{ m}$
Nested volume element	
Ratio of volume	Fracture : Matrix1 : Matrix2 = 0.02 : 0.2 : 0.78
Relative Permeability	
Corey curves	$S_{lr} = 0.30, S_{sr} = 0.10$

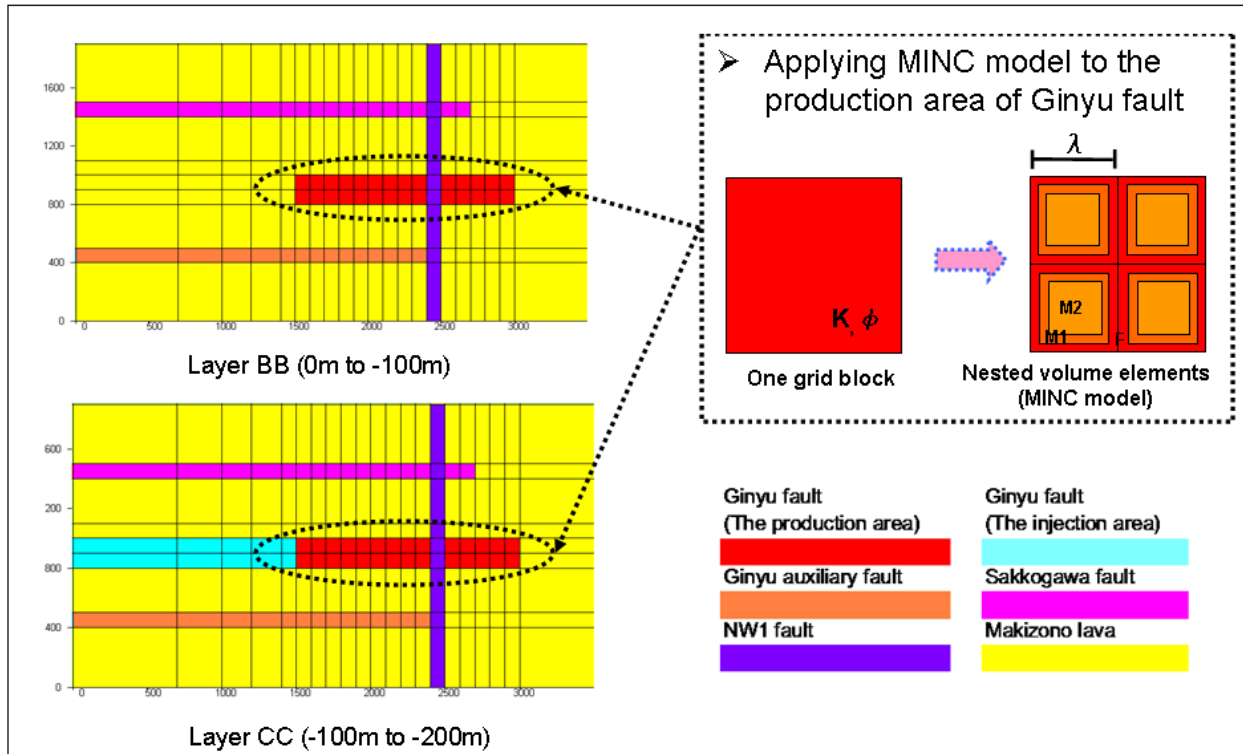


Figure 5: Area applied MINC method in the numerical model for the Ogiri geothermal field

#### 4-3. Analysis conditions for simulation

We carried out history-matching simulations with the model that locally assigns the MINC method to BB and CC layers at Ginyu Fault zone. The calibration period is 22 years from July 1984 to August 2006. For the initial condition of the numerical model, the natural state model for the Ogiri geothermal field obtained through the preexploitation modeling was employed (Kumamoto et al., 2008b). For the boundary conditions of the model, constant pressure of  $9.807 \times 10^4$  Pa and temperature of  $75^\circ\text{C}$ . at the top surface was given. The lateral boundaries were assumed to be impermeable with respect to mass and adiabatic to heat and large volume blocks were assigned along periphery of the model. The conductive heat flux of  $0.432 \text{ W/m}^2$  was assigned to the grid blocks of the bottom layer on the southern part of Sakkogawa Fault. The remaining bottom layer blocks were assigned with that of  $0.0432 \text{ W/m}^2$ . Moreover, mass recharge was specified at two blocks of the bottom layer. Mass of  $30 \text{ kg/s}$  of  $1047.1 \text{ kJ/kg}$  for a grid block located in the eastern part was assigned and mass of  $55 \text{ kg/s}$  of  $1062.7 \text{ kJ/kg}$  was recharged into the other block located in deep zone of the production area. Therefore, the total mass of  $85 \text{ kg/s}$  of about  $240^\circ\text{C}$  water was recharged at depth into the model during the exploitation stage. The flow-rate histories of the produced fluid and reinjected water were used as sink/source. Figure 6 shows the histories of production and reinjection flow rates. Low temperature reinjection water of  $546.3 \text{ kJ/kg}$  (saturated water of  $130^\circ\text{C}$ ) was reinjected on the basis of the actual operating condition. During history matching simulation, the simulated results were compared against measured temperature and pressure histories in the two observation wells of KE 1-19 and KE1-13. Moreover, measured flowing enthalpy histories in the 13 production wells were compared with simulated values.

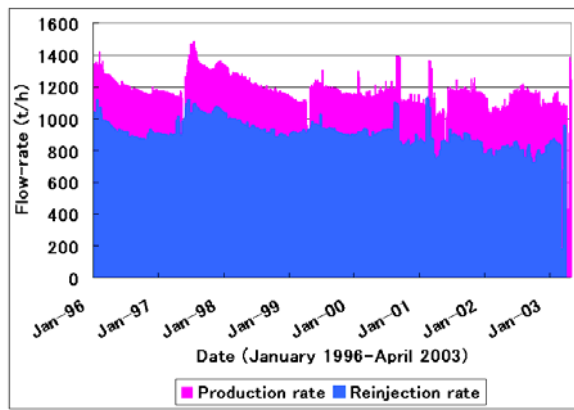


Figure 6: Flow-rate histories of produced and reinjected water

#### 5. RESULTS AND DISCUSSION

Simulated pressure and temperature histories are compared against the measured values in two observation wells, KE1-19 and KE1-13. Their pressure and temperature histories after 1995 when full production operation started seem to represent pressure and temperature in the hot-water dominated zone and in the two-phase zone, respectively. In particular, the relationship between pressure and temperature in Well KE1-13 after 1995 can be plotted on those of saturated water, thus the well represents pressure and temperature of steam-water two-phase zone.

Figure 7 shows comparison among measured and computed pressure and temperature transients in Well KE1-13 together with simulated results with the porous model (Kumamoto et al. 2008b). Before starting the full production in 1995, simulated pressures show similar values among the models. However, quick decreases occurs after 1995 followed by the full production and their discrepancies grow with time. This quick drops in pressure likely lead formation of two-phase zone in shallow layers where Well KE1-13 locates. Simulated temperatures also show a similar behavior as those of pressure history.

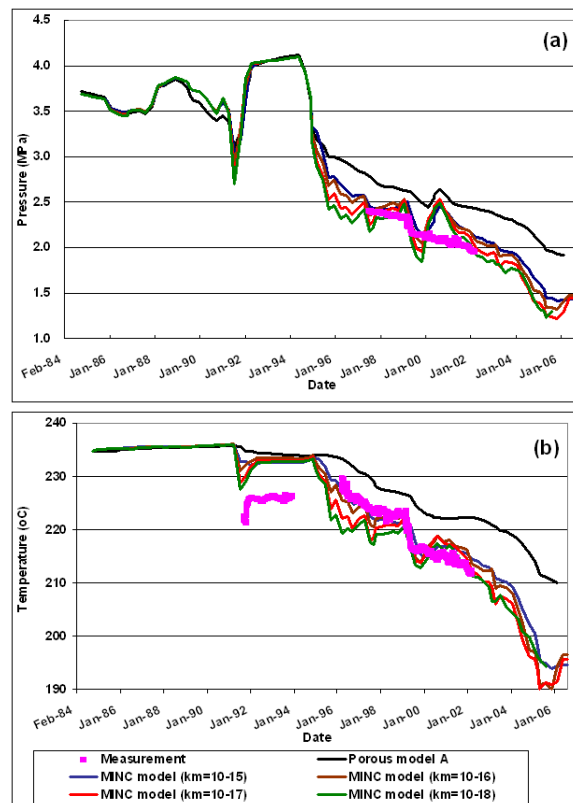


Figure 7: Simulated pressure (a) and temperature (b) transients in Well KE1-13 through history matching simulation

In order to examine the differences of computed results among the porous and MINC models, the history matching simulation results between 1995 and 2006 are extracted as shown in Figure 8. Simulated pressure and temperature transients with the MINC models generally provide better matches with measurements compared to those with the porous model.

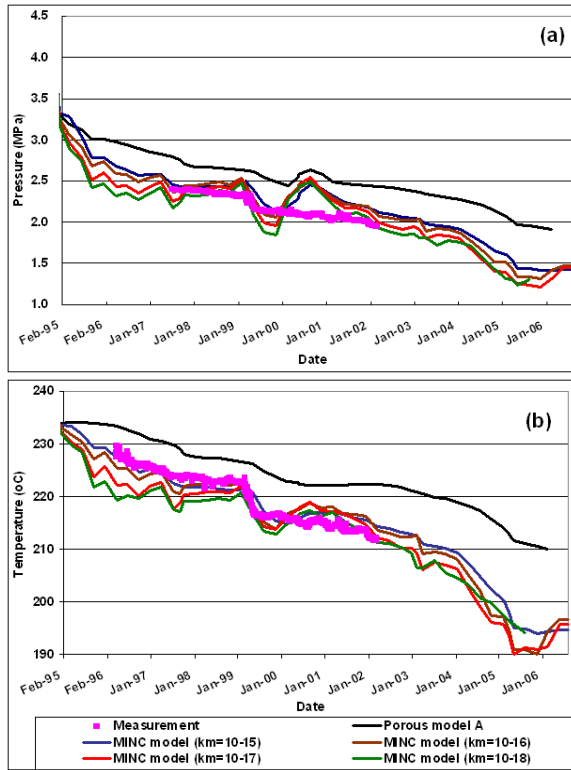


Figure 8: Simulated pressure (a) and temperature (b) histories in Well KE1-13 during full mass production

The simulated temperature history with the MINC model with  $k_m=10^{-15} \text{ m}^2$  shows the better matches with the measurements. The discrepancies between the calculations and measurements are within 3 °C. On the other hand, the computed temperatures with the MINC models with small values  $k_m$  decrease more quickly with time. The differences between simulated and measured ones are within 5 °C and the discrepancies are conspicuous in the early time soon after the full production started. This is considered that supply of fluid from matrix to fracture space is small for low  $k_m$  in early times of fluid production in 1995-1997, and result in fasten decrease in both pressure and temperature. However, as time passes, these discrepancies become small. The computation with the MINC model of  $k_m=10^{-18} \text{ m}^2$  and with porous model could not continue after March 2006 because of marked decreases in pressure and

temperature in the grid block where fluid production is assigned. This grid block resulted in a full depletion of fluid in the grid element. Other MINC models with high  $k_m$  succeeded in computation.

Measured enthalpy histories in 13 production wells are used to compare with simulated values through the history matching simulation.

Figure 9 shows comparison of simulated and measured enthalpies of Well A2 and A3. Feed zones of these wells locate in the deep hot-water dominated zone. As can be seen, simulated enthalpies remains about 1000 kJ/kg throughout the simulation period and no distinct difference due to values of  $k_m$  can be seen.

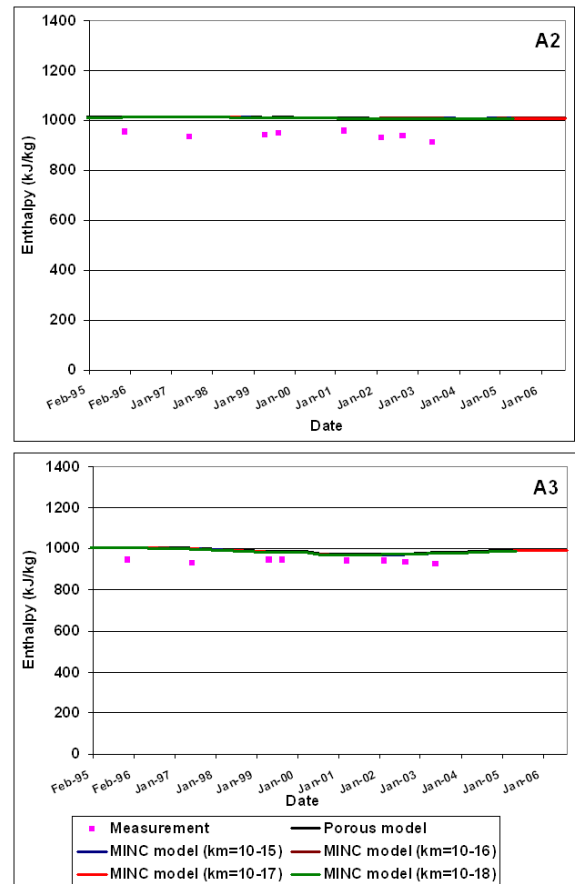


Figure 9: Comparison between measured and simulated enthalpy histories of Wells of A2 and A3

Figure 10 shows a comparison of measured and simulated enthalpy histories of Well C1. The well starts producing high enthalpy fluid soon after the full production and produces dry steam. Thus, we can

say that the feed zone of Well C1 presents the vapor-dominated two-phase zone. Simulated results with MINC model of  $k_m=10^{-18} \text{ m}^2$  show quick increases with time soon after the full production in 1995, and also show higher enthalpy values compared with other MINC models. However, their differences gradually decrease with time. Then, the computed results with MINC models having different  $k_m$  show similar changes with time from 1999 to 2000 though there are small discrepancies. In the later period of history, the simulated results with the MINC model having low  $k_m$ ,  $10^{-17} \text{ m}^2$  and  $10^{-18} \text{ m}^2$ , present large fluctuations. Then, the simulation could not be continued further for the cases with  $k_m = 10^{-18} \text{ m}^2$  and the porous model. This is because pressure of grid block where the production is assigned dropped quickly due to depletion of fluid. The simulated enthalpy history with the porous model tends to show the lowest values throughout the simulation period. Although simulated results with MINC models show the higher values compared with those with the porous model, we could not obtain reasonable matching results between simulated and measured enthalpy histories.

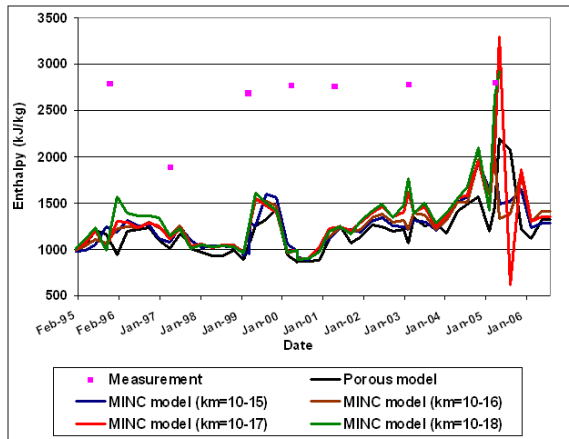


Figure 10: Comparison between measured and simulated enthalpy histories of well C1

The contour map of the simulated vapor distribution with the MINC model having  $k_m = 10^{-15} \text{ m}^2$  is depicted in Figure 11. The two-phase zone with high vapor saturation extends along the production area of Ginyu Fault. On the other hand, the contour map of computed results with the porous model shows relatively lower vapor saturation.

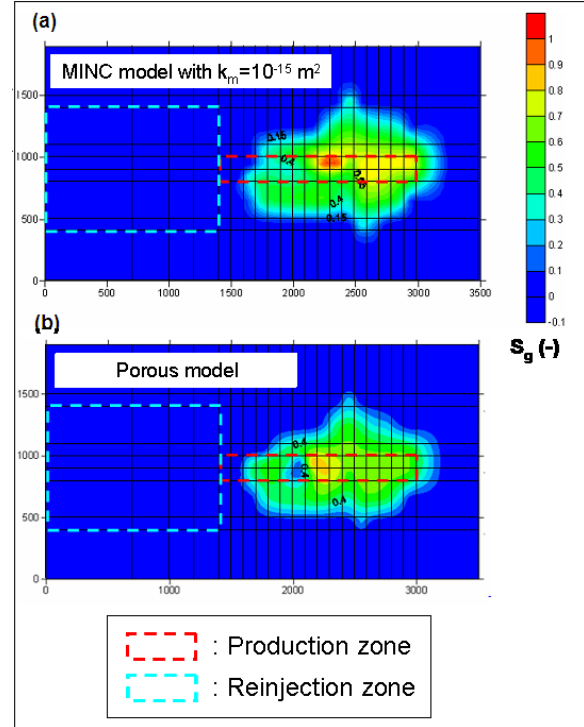


Figure 11: Plan view of simulated vapor saturation in the layer BB in 2006. (a) and (b) show simulated results with the MINC model with  $k_m = 10^{-15} \text{ m}^2$  and with the porous model, respectively

## 6. CONCLUSIONS

A numerical model of the fractured geothermal reservoir for the Ogiri field was developed by applying the MINC method. The history matching simulations with the model were conducted with the code TOUGH2. The results can be summarized as follows:

1. The MINC models with the matrix permeability of  $k_m=10^{-15} \text{ m}^2$  provided the best match between the measured and simulated pressure and temperature transients of Well KE1-13 that locates in steam-water two-phase zone.
2. Good match was not obtained with the MINC models for enthalpy history of Well C1 that produces dry steam.

## ACKNOWLEDGEMENTS

We would like to thank Dr. K. Goko and Mr. T. Horikoshi for valuable discussions and comments. Thanks also go to Nittetsu Kagoshima Geothermal Co. for permission to publish their data and for their support. Finally, special thanks go to Prof. Roland N. Horne and Stanford Geothermal Program for their support to attend the 34<sup>th</sup> Stanford Geothermal Workshop.

## **REFERENCES**

Finsterle, S. (2000), "iTOUGH2 User's Guide," *Report LBNL-40040 Updated Reprint*, Earth Sciences Division, Lawrence Berkeley National Laboratory, University of California, Berkeley, CA 94720.

Goko, K. (1995), "Geological analysis and evaluation of the Ogiri geothermal structure in the Kirishima geothermal area," *Resource Geology (in Japanese with English abstract)*, **45**, 41-52.

Goko, K. (2000), "Structure and hydrology of the Ogiri field, West Kirishima geothermal area, Kyushu, Japan," *Geothermics*, **29**, 127-149.

Goko, K. (2004), "Towards Sustainable Steam Production; the Example of the Ogiri Geothermal Field," *Journal of the Geothermal Research Society of Japan (in Japanese with English abstract)*, **26**, 151-164.

Imura, R. and Kobayashi, T. (2001), "Geological Map of Kirishima Volcano 1:50,000," Geological Map of Volcanoes, 11., Geological Survey of Japan.

Japan Geothermal Energy Association. (2000), "Directory of Geothermal Power Plant in Japan (New Edition)," *Japan Geothermal Energy Association (in Japanese)*, 254pp.

Kodama, M. and Nakajima, T. (1988), "Exploration and Exploitation of the Kirishima Geothermal Field," *Journal of the Japan geothermal Energy Association (in Japanese with English abstract)*, **25**, 1-30.

Kumamoto, Y., Itoi, R., Tanaka, T. and Hazama, Y. (2008), "Development of the Optimum Numerical Reservoir Model of the Ogiri Geothermal Field, Kyushu, Japan, Using iTOUGH2," *Proc. of 33rd Workshop on Geothermal Reservoir Engineering*, Stanford University, CA USA, CD-ROM.

Kumamoto, Y., Horne, R. N., Itoi, R., and Hazama, Y. (2008), "Numerical modeling of the Ogiri geothermal system, Kyushu, Japan," *Transactions of Geothermal Resources Council*, **32**, 449-458.

NEDO (New Energy Development Organization). (1983), "Geothermal Development Promotion Survey Report, No 3, Kurino and Mitarai Area," *New Energy Development Organization (in Japanese)*, pp. 1 - 135.

NEDO. (1987), "Nationwide geothermal resources exploration project (2nd stage). Volcano-related hydrothermal convection system type, Kokubu area, volcano-geothermal map of Kokubu area and

compiled geological map of Kokubu geothermal area," *New Energy Development Organization (in Japanese)*, pp. 1-67.

O'Sullivan, M. J. and Bullivant, D. P. (1995), "A graphical interface to the TOUGH2 family of flow simulators," *Proc. of TOUGH Workshop 1995*, Lawrence Berkeley Laboratory Report LBL-37200, CA USA, 90-95.

Pruess, K. (1983), "Heat Transfer Fractured Geothermal Reservoirs With Boiling," *Water Resources Research*, **19**, 201-208.

Pruess, K., Oldenburg, C. and Moridis, G. (1999), "TOUGH2 USER'S GUIDE, VERSION 2.0," *Report LBNL-43134*, Earth Sciences Division, Lawrence Berkeley National Laboratory, University of California, Berkeley, California 94720.

Taguchi, S., Okaguchi, M. and Yamasaki, M. (1983), "Fission track ages of some volcanic rocks from the Kirishima geothermal region," *Report of Research Institute of Industrial Science, Kyushu University (in Japanese with English abstract)*, **74**, 49-54.